

# Demonstration of the Application of the Total Focusing Method to the Inspection of Steel Welds

Matthias JOBST, George D. CONNOLLY, GE Sensing & Inspection Technologies GmbH,  
Hürth, Germany

**Abstract.** Ultrasonic phased arrays offer many advantages for industrial inspection due to increased flexibility over methods involving single-element probes. This paper will compare and contrast two previously-developed methods for the inspection of welds involving phased arrays: the swept sector scan and the total focusing method, with particular emphasis on the latter. The total focusing method requires the acquisition of the full data set of time-domain signals from every possible send-receive combination in an ultrasonic array and the computation of time delay laws that will allow focusing at the post-processing stage. Two variations of the total focusing method are also presented: the common source method and the synthetic aperture focusing technique. These variations are discussed and their use for weld inspection is investigated. The resulting images from experiments involving an aluminium block with side-drilled holes and industrial weld samples containing various realistic defects are shown.

## 1. Introduction

In recent years, phased array (PA) techniques are finding increasing numbers of applications for the inspection of industrial components. Amongst their advantages over conventional inspection are the following [1]:

- With the application of steered beams, inspection is potentially a much more rapid process
- Ultrasonic images are easy to understand and minimal operator training is needed for their interpretation
- Flaws can be located directly and immediately evaluated
- Multiple types of inspection may be performed with the same equipment by adjusting the relative time or amplitude with which the elements introduce the signal
- They present the possibility of volumetric imaging through the generation of 3D images of the specimen interior

A clear image of the interior of a specimen requires the focusing of sound energy to a focal point. The focusing may be performed either at the transmission stage, where the appropriate delay laws are applied such that each element pulses at a slightly different time to steer the energy towards a point; or focusing may be applied synthetically by shifting and sampling the A-scans after reception at the post-processing stage. If the full matrix capture data are used, then this method is called the total focusing method (TFM).

Literature studies [2] have shown this method to have the highest array performance amongst PA techniques due to superior focusing. It has been described as the "gold standard" [3] to which other methods can and should be compared.

## 2. Inspection methods

### 2.1 TFM Overview

In the paper, we will apply TFM only to cross-sections of material, focusing on a series of points arranged in a grid of  $n_x$  and  $n_y$  points as shown in Fig. 1.

The TFM requires the extraction of the maximum amount of possible information from the specimen. If we have an array of  $n_e$  elements, then we will have each element activated one after the other, and all elements will receive independently. The relevant data from the complete send-receive combination will lie in a matrix of size  $n_e \times n_e \times n_s$  where  $n_s$  is the number of time samples in each signal. However, we will represent the data as a matrix  $\mathbf{S}_{ij}(t)$  for  $1 \leq i \leq n_e$  and  $1 \leq j \leq n_e$ .

Delay laws are unique to each focal point in the grid. The matrix containing the laws for the entire area of interest in the specimen will be of size  $n_x \times n_y \times n_e$  and will be called  $\mathbf{D}_{ikl}$  for  $1 \leq i \leq n_e$ ,  $1 \leq k \leq n_x$  and  $1 \leq l \leq n_y$ .

The array is focused on every point in the image in turn through both reception and transmission in the following manner to produce an image matrix  $\mathbf{I}$ :

$$I_{kl} = \left| \sum_i \sum_j S_{ij} (\mathbf{D}_{ikl} + \mathbf{D}_{jkl}) \right| \quad (1)$$

### 2.2 Variations of TFM

Two variations of TFM will be introduced here. The first is the Common Source Method (CSM). The difference with TFM is that the CSM algorithm has no dependency on source element since the source is common to all acquired data scans, whose matrix will now take the form  $\mathbf{S}_j(t)$ , the index  $j$  denoting the index of the receiving element. The image matrix is produced from the expression

$$I_{kl} = \left| \sum_j S_j (\mathbf{D}'_{kl} + \mathbf{D}_{jkl}) \right| \quad (2)$$

where  $\mathbf{D}'_{kl}$  indicates the delay laws for the common source, which depend only on the location of the image point. The second is the Synthetic Aperture Focusing Technique (SAFT), also known as the Back-Scatter Method. It varies with respect to TFM in that the only element that receives is also the one that sends. The data set can thus be written as  $\mathbf{S}_i(t)$  where  $i$  denotes the index of the sending element. The corresponding algorithm for the generation of the image is

$$I_{kl} = \left| \sum_i 2S_i (\mathbf{D}_{ikl}) \right| \quad (3)$$

Thus all three methods vary only with respect to their send-receive combinations, as shown in Fig. 2. The variants need a number of calculations of  $O(n_e)$  and so are capable of generating an image in a shorter period of time since TFM uses  $O(n_e^2)$  calculations. The CSM also offers a much faster acquisition time, requiring only one cycle whereas both SAFT and TFM need  $n_e$  cycles. The theoretical resolution of CSM and SAFT images are lower than those of TFM [4], partly because a greater amount of data are acquired thus lowering the effects of noise.

### 2.3 Delay law computation

In this section the computation of the delay law matrix  $\mathbf{D}_{ikl}$  is shown. This involves the tracing of a ray joining the centre of the array element to the image point. Here reciprocity is assumed, where the time taken for the ray to travel from the element to the image point is the same if the direction were reversed. Let us assign the co-ordinates  $(x_e, y_e)$  to the centre of the element and the co-ordinates  $(x_p, y_p)$  to the image point.

If there are no interfaces present in the model (a schematic is shown in Fig. 3(a)), the propagation time  $t$  is

$$t = c\sqrt{h_1^2 + v_1^2} \quad (4)$$

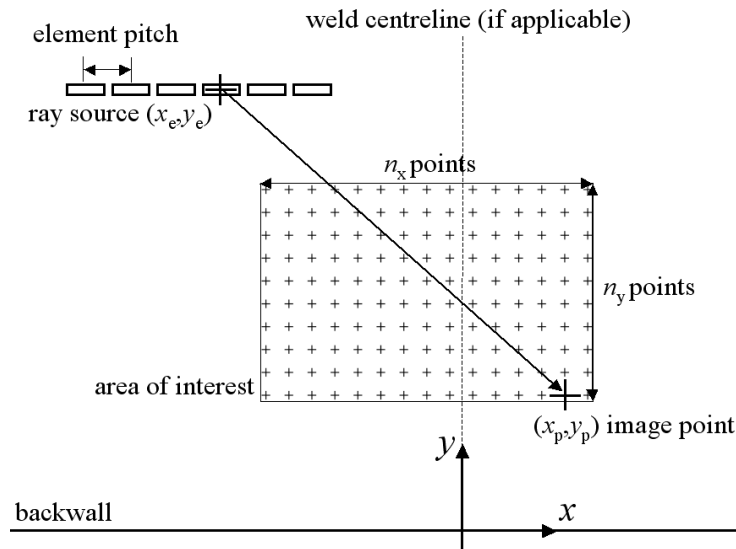


Fig. 1. General schematic diagram of TFM

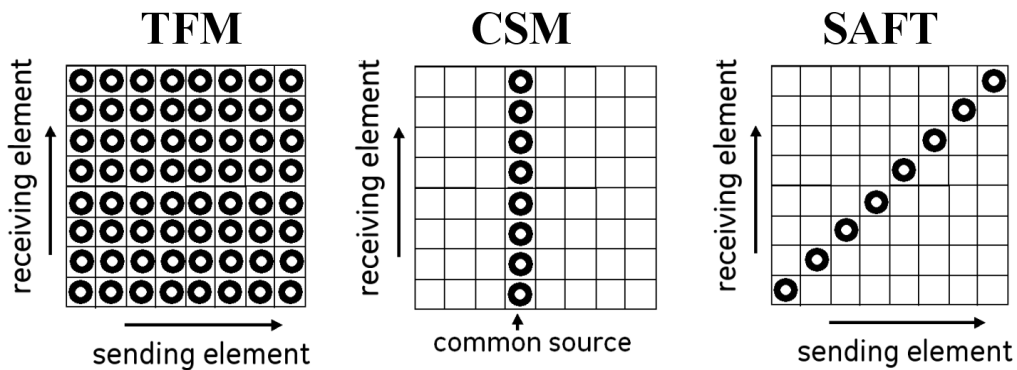


Fig. 2. Send-receive combinations of the three imaging algorithms

with  $h_1 = |x_e - x_p|$ ,  $v_1 = |y_e - y_p|$  and  $c$  as the sound velocity. If the inspection setup involves a wedge (Fig. 2(b)) or backwall reflection (Fig. 3(c)), then the propagation time will be

$$t = c_1 \sqrt{h_1^2 + v_1^2} + c_2 \sqrt{h_2^2 + v_2^2} \quad (5)$$

where the ray velocities in the upper and lower materials are  $c_1$  and  $c_2$  respectively, the ray intersects the interface at  $(x_1, y_1)$  and the other values are as defined in Fig. 3(b) and Fig. 3(c). The value of  $y_1$  is known *a priori* though the value of  $x_1$  is not. It may be calculated thus:

$$x_1 = x_e + r \quad (6)$$

where  $r$  is the positive real root of the following polynomial equation in  $a$ :

$$a^4(c_2^2 - c_1^2) + 2a^3(h_1 + h_2)(c_1^2 - c_2^2) + a^2[c_2^2((h_1 + h_2)^2 + v_2^2) - c_1^2((h_1 + h_2)^2 + v_1^2)] + 2ac_1^2v_1^2(h_1 + h_2) - c_1^2v_1^2(h_1 + h_2)^2 = 0 \quad (7)$$

Delay laws are presented visually in Fig. 4 for the inspection of an aluminium specimen, using a variety of wave modes. In these examples, the area of interest extends below the backwall, showing that this method may be extended to include half-skip and full-skip inspection types.

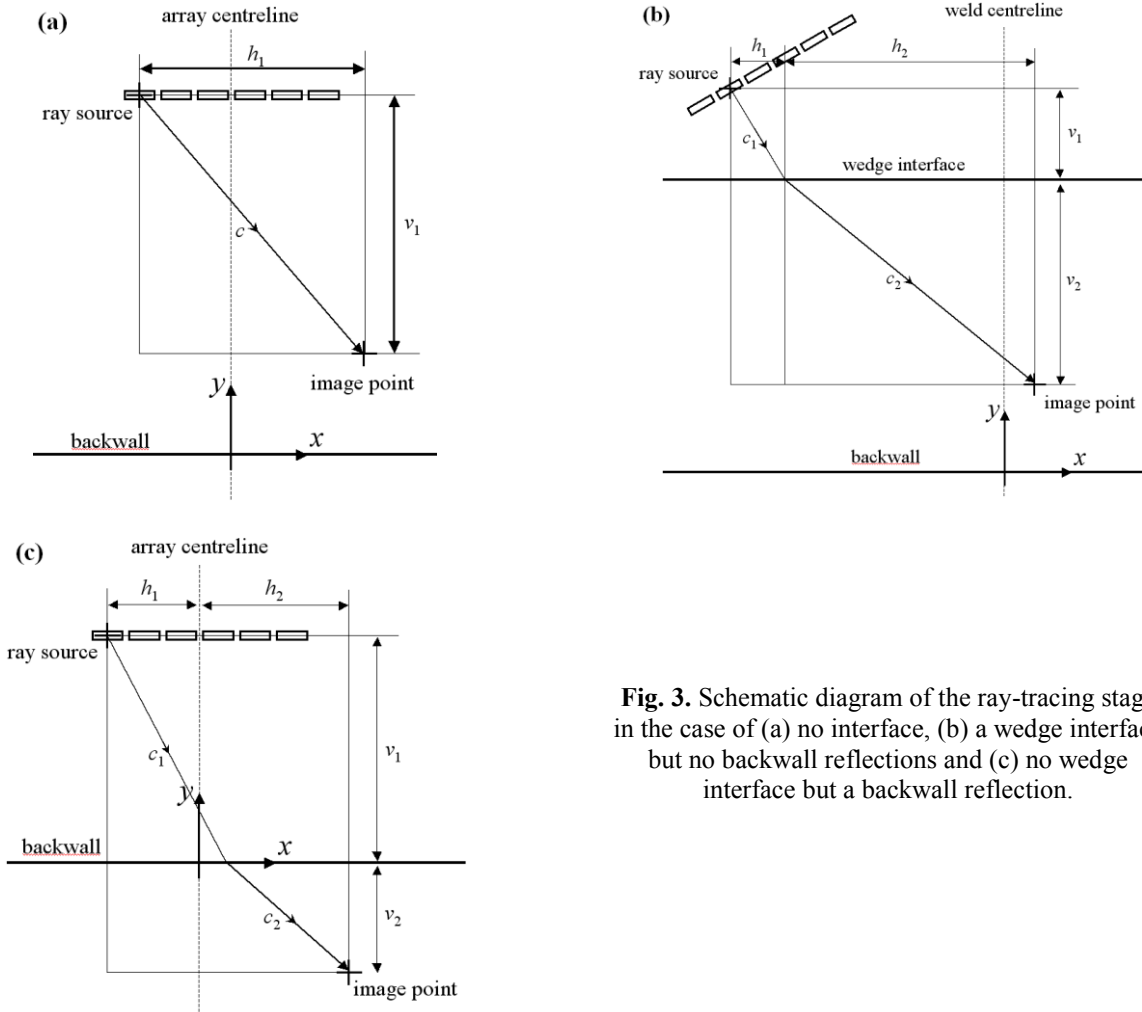


**Fig. 3.** Schematic diagram of the ray-tracing stage in the case of (a) no interface, (b) a wedge interface but no backwall reflections and (c) no wedge interface but a backwall reflection.

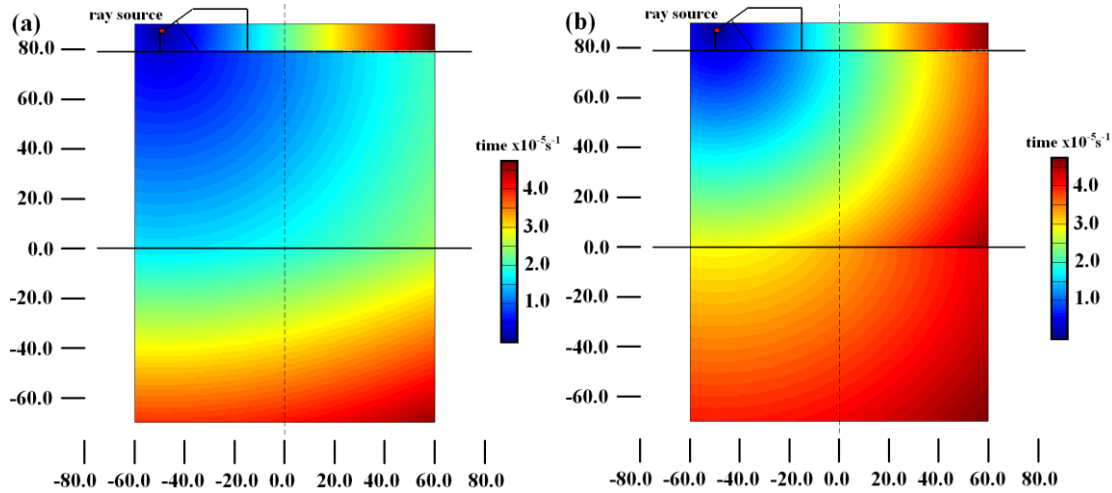


**Fig. 4.** Visual representation of delay laws (arbitrary centreline position) plotted according to image point position for a polystyrene wedge to inspect an aluminium block of 79mm thickness using (a) longitudinal waves that convert to transverse waves and (b) transverse waves that convert to longitudinal waves upon reflection at the backwall.

#### 2.4 Swept sector scans

Sector scans make use of all the elements in the array to steer the beam but do not use focusing. Typically, all elements will receive at the same time and what they have recorded will be combined into a single A-scan. The values in this A-scan will be drawn on the screen at the appropriate angle. Like the TFM image, the sector scan is to-scale and thus corresponds directly to the cross-section of the test piece.

#### 2.5 Measurement of performance

A quantitative method of measuring sharpness of focusing will be introduced to aid the comparison between different images. The method used in this paper will be that previously used by Holmes et al. [5]. The measured area of the indication corresponding to a particular defect at  $-6\text{dB}$  will then be normalised according the wavelength of the centre frequency to give an API value:

$$\text{API} = \frac{\text{area}_{-6\text{dB}}}{\lambda^2} \quad (8)$$

A smaller number indicates a sharper focus and superior performance.

### 3. Experimental procedure

Tests have been performed on one block of aluminium and two steel weldments with various prepared defects. The aluminium block measures  $143\text{mm} \times 78\text{mm} \times 49\text{mm}$  and has 25 side-drilled holes of 1mm diameter in a band and an arc. It also has 24 holes of 0.8mm diameter towards one of the corners. All the holes are 20mm deep. Scans on this block did not use a wedge.



**Fig. 5.** The Phasor XS

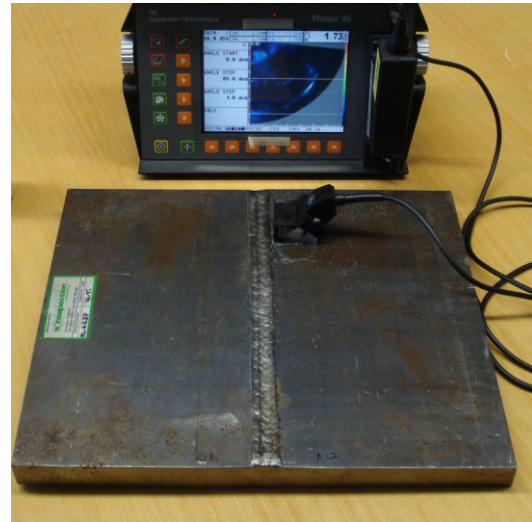


**Fig. 6.** Inspection of prepared welds

The steel weldments have dimensions 334mm×300mm×24mm. One contains an X-weld that is 18mm wide at the top and the bottom faces, and the other contains a V-weld that measures 32mm and 4mm at the widest and narrowest points respectively. Wedges of 36° were used on both weld scans.

Additionally, TOFD scans were carried out on the welds in order to aid the decision as to where along the weld the PA and TFM scans would be carried out. The TOFD scans were made using probes of 5MHz centre frequency manufactured by Imasonic (Besançon, France) housed in 60° wedges and the image generation was performed by GEIT MapStar [6] and GEIT UltraMap [7]. The instrument used to acquire data in both cases and to produce sector scan images was the Phasor XS (Fig. 5), the Universal Flaw Detector from GE Inspection Technologies. The wedges were positioned to face the weld directly (see Fig. 6) and the distance from the weld centreline was adjusted to receive the clearest possible sector scan images. The TFM images were compiled from data received from exactly the same array position for direct comparison.

## 4. Experimental results

### 4.1 Aluminium block

Scans were made on the aluminium block using an array with a pitch of 0.5mm containing 32 elements, though the hardware would only allow a 16 element aperture for the sector scan. The array introduced longitudinal waves into the specimen and reflected signals were plotted to a swept sector scan from  $-60^\circ$  to  $+60^\circ$ . Results on the aluminium block from various positions along its surface invariably showed that the TFM offered greater image resolution. The images from one such example are shown in Fig. 6. It can clearly be seen that the arc reflectors away from the centreline are difficult to resolve in the sector scan (Fig. 7(b)) whereas the TFM image (Fig. 7(c)) allows the viewer to completely resolve all 16 holes. The API values for the holes are shown in Fig. 7(d) only where it was possible to calculate them. Given that all side-drilled holes are of the same size, it can be seen that array performance decreases when the reflector is farther away from the array and at a greater angle to the array centreline. The quality of the TFM image holds well enough for reflectors to be resolved even at angles of  $65^\circ$  or higher.



signals will be strong enough to draw a duplicate image of the defect to the screen. The TFM does not suffer to the same degree since the delay laws are computed with the wave velocities corresponding to only one wave mode thus strongly weakening all other wave modes during the focusing stage.

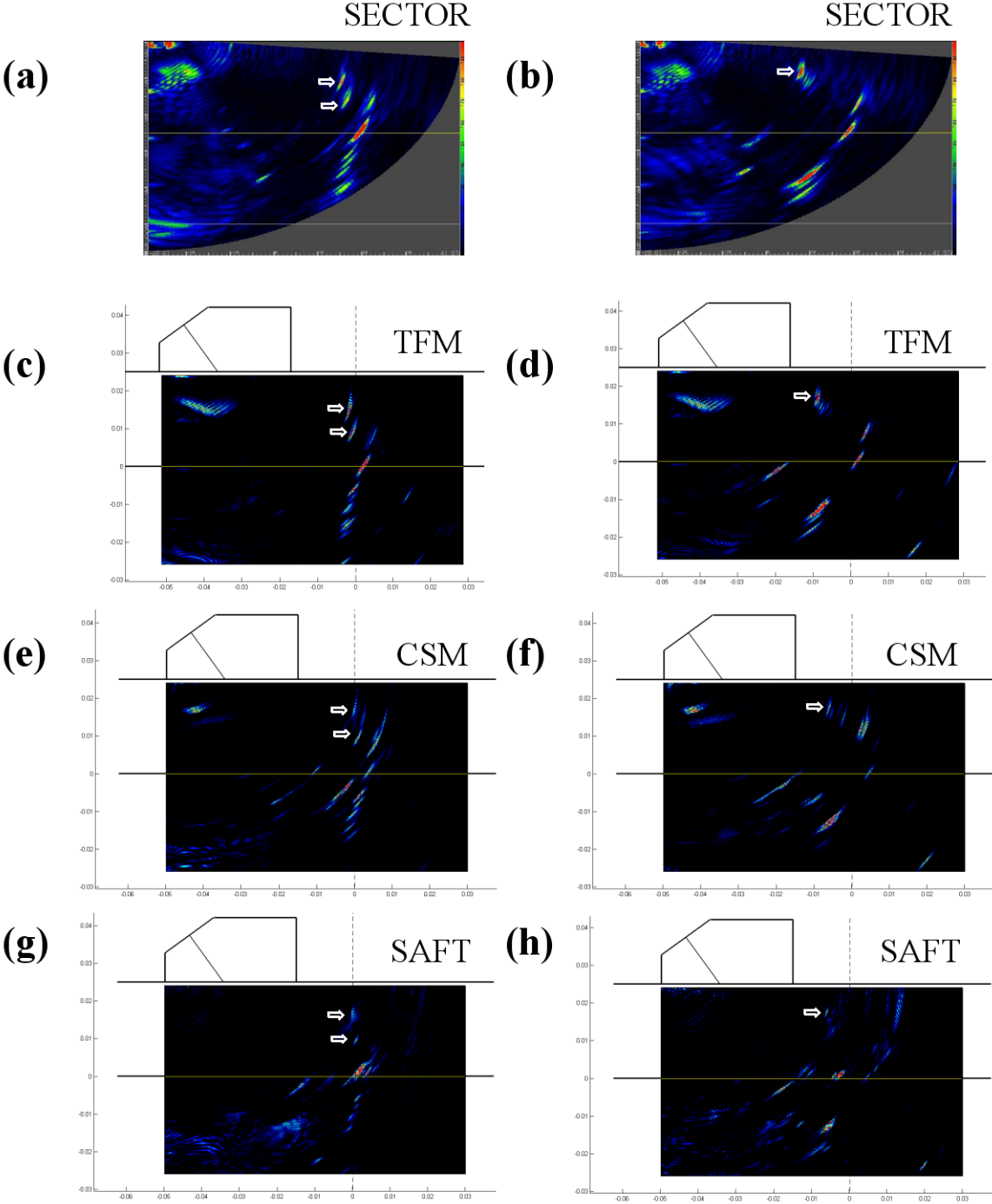


**Fig. 8.** Image comparisons from the V-weld: those on the left column image the centreline crack and those on the right column image the side wall crack. Dotted line indicates the centreline of the weld. Arrows point to significant indications.

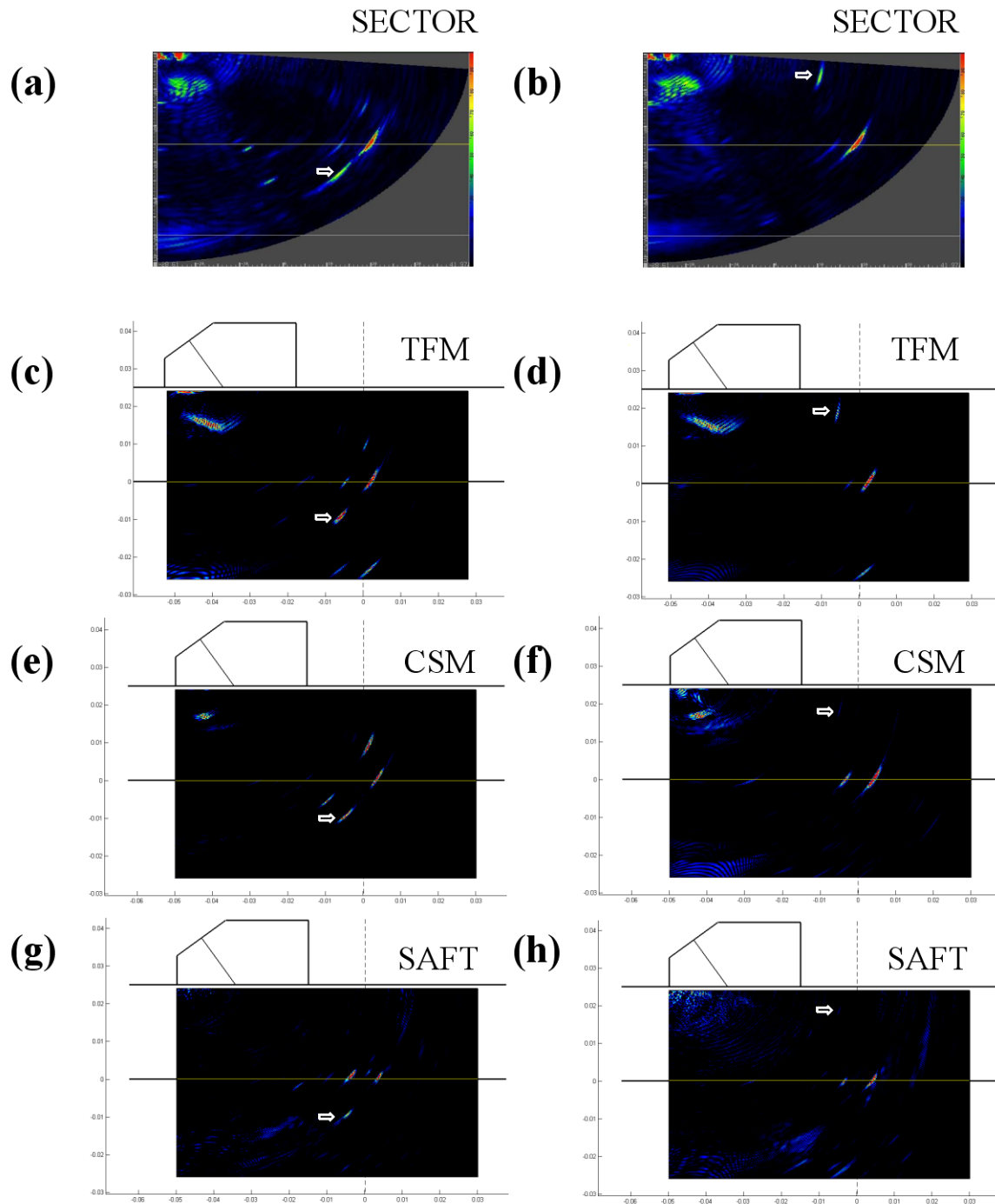


**Fig. 9.** Image comparisons from the X-weld: those on the left column image the centreline crack and those on the right column image the side wall crack. Dotted line indicates the centreline of the weld. Arrows point to significant indications.

The CSM and SAFT imaging algorithms are affected by poor image quality to varying degrees due to the smaller data set available for the focusing process. Thus their images may show unwanted features near the wedge other than the reflection of the array face about the wedge-weldment interface (e.g. Fig. 9(h)) or in reflected space (e.g. Fig. 9(g)), indications may be more elongated (compare Figs 8(c) and 8(e)) or array performance may be poorer at high angles away from the beam centre (e.g. slag indication in Fig. 9(d) much stronger than those in Figs 9(f) and 9(h)).

**Table I.** API values for weld indications

Weld type	Defect in image	Indication	API value
V	Centreline crack	Bottom right weld corner	3.80
		Centreline crack (top)	5.70
		Centreline crack (bottom)	3.87
	Side wall crack	Bottom right weld corner	2.98
		Crack (nearer end)	3.39
X	Incomplete root (centre)	Bottom left weld corner	4.20
		Bottom right weld corner	4.27
		Incomplete root (direct)	4.54
		Incomplete root (full-skip)	5.36
	Slag	Bottom left weld corner	3.59
		Bottom right weld corner	4.75
		Slag	4.81

## 5. Discussion and perspectives

It has been seen that a method of data extraction for every possible send-receive combination of the phased array has been successfully implemented. Tools that generate delay laws offline and their use to focus these extracted data have also been demonstrated experimentally and the results are comparable or, in some cases, superior to those generated through the swept sector scan. The imaging process has been shown for cases both with and without a wedge attached to the array.

The general issue of weaker signal penetration as compared to the sector scan could be alleviated by averaging the recorded A-scans over time for each element in turn to increase the signal to noise ratio though this would be done at the expense of acquisition speed. It would also be possible to inspect the specimen with either larger elements or to use sub-arrays to increase the amount of energy introduced into the structure with every cycle, or to consider the use of alternative techniques, such as the Retrospective Transmit Focus [8].

The TFM has two benefits over sector scan that are visible from the presented results:

- Superior array performance due to superior focusing algorithm (Fig. 6(c)) as compared to the sector scan, which uses divergent beams
- Less susceptible to interference due to other wave modes since delay laws are particular to a single specified wave mode (Figs 8 and 9)

This method also has the following practical advantages over sector scan:

- With hardware that would accommodate an independent channels for each array element, it would be quicker to acquire data to generate a TFM image than a typical sector scan. A TFM acquisition would need a number of cycles equal to the number of elements in the array whereas a sector scan still needs one cycle for each angle step
- The auditable nature of the acquired data allows the drawing of many other types of image, including conventional scans. If time is an important factor, one may elect for a more rapid algorithm to be employed such as the CSM or SAFT [3]. Either of these algorithms will allow an increase in drawing speed of a factor equal to the number of elements in the array, at the cost of poorer image quality as demonstrated in this paper. If image quality is more important, then TFM could be applied from the same dataset. Thus data do not have to be reacquired in order to create a different type of image.

## References

- [1] Berke, M. and Büchler, J. Ultrasonic imaging in automatic and manual testing. ECNDT 2006 – We.3.1.5
- [2] Hunter, A.J., Drinkwater, B.W. and Wilcox, P.D. The wavenumber algorithm for full-matrix imaging using an ultrasonic array. *Ultrasonics, Ferroelectrics and Frequency Control*, IEEE Transactions on, 2008; 55(11):2450-2462
- [3] Thomenius, K. Evolution of Ultrasound Beamformers, *IEEE Ultrasonics Symposium*, 1996; 2, 1615-1622
- [4] Chiao, R.Y. and Thomas, L.J. Analytical evaluation of sampled aperture ultrasonic imaging techniques for NDE. *Ultrasonics, Ferroelectrics and Frequency Control*, IEEE Transactions on, 1994; 41(4):484-493
- [5] Holmes, C., Drinkwater, B.W. and Wilcox, P.D. Post-processing of the full matrix of ultrasonic transmit-receive array data for non-destructive evaluation. *NDT&E International*, 2005; 38:701-711
- [6] GE Inspection Technologies MapStar UT URL:  
[http://www.geinspectiontechnologies.com/en/products/ut/system\\_instrumentation/mapstarut.html](http://www.geinspectiontechnologies.com/en/products/ut/system_instrumentation/mapstarut.html)
- [7] GE Inspection Technologies UltraMAP weld software URL:  
[www.krautkramer.ipc.ru/Docs/portable\\_flaw\\_detectors/UltraMap2.pdf](http://www.krautkramer.ipc.ru/Docs/portable_flaw_detectors/UltraMap2.pdf)
- [8] Bradley, C. Retrospective Transmit Beamformation, ACUSON SC2000 Volume Imaging Ultrasound System. Available online, URL:  
[www.medical.siemens.com/siemens/sv\\_SE/gg\\_us\\_FBAs/files/misc\\_downloads/Whitepaper\\_Bradley.pdf](http://www.medical.siemens.com/siemens/sv_SE/gg_us_FBAs/files/misc_downloads/Whitepaper_Bradley.pdf)